Mineral Snowflakes on Gas-giant and Ultra-hot Exoplanets

Dominic Samra [1,2] Christiane Helling [1,2,3] Michiel Min [3,4] Til Birnstiel [5]

(1) Centre for Exoplanet Science, University of St Andrews; (2) SUPA, School of Physics & Astronomy, University of St Andrews; (3) SRON Netherlands Institute for Space Research; (4) Astronomical Institute Anton Pannekoek, University of Amsterdam; (5) University Observatory, Faculty of Physics, Ludwig-Maximilians-Universität

3rd Year PhD Student
University of St Andrews
Website: dominicsamra.uk
Email: dbss3@st-andrews.ac.uk

Introduction

Clouds have a major impact on gas-giant exoplanet atmosphere observations. The details of cloud particle formation become increasingly important with the next generation of telescopes and instruments (e.g. JWST). We investigate the impact of collisons between cloud particles on the cloud population, as well as the formation of non-compact and non-spherical clouds for a 'Typical Warm Gas Giant atmosphere'. We then apply a model for irregularly shaped cloud particles for gas-giant WASP-43b ($T_{\rm eff} \approx 1700\,{\rm K}$ [1]) and ultra-hot jupiter HAT-P-7b ($T_{\rm eff} \approx 2200\,{\rm K}$) [2]. The work presented here is expanded upon significantly in three puplished papers, and one further in preparation:

- Mineral snowflakes on exoplanets and brown dwarfs: Effects of micro-porosity, size distributions, and particle shape [3]
- Understanding the atmospheric properties and chemical composition of the ultra-hot Jupiter HAT-P-7b; I. Cloud and chemistry mapping [4]
- Mineral cloud and hydrocarbon haze particles in the atmosphere of the hot Jupiter JWST target WASP-43b [5]

Irregularly Shaped Particle Model

We model non-compact particles by introducing a constant parameter $f_{\rm por}$ such that the effective material $\rho_{\rm s}^{\rm eff}$ is $\rho_{\rm s}^{\rm eff} = \rho_{\rm s}(1 - f_{\rm por})$. Heterogeneous cloud particle opacities are calculated with Mie theory [6], and effective medium theory (EMT) with the Bruggeman mixing rule [7]. Micro-porosity is incorporated as vacuum (refractive indices $n = 1$, $k = 0$).

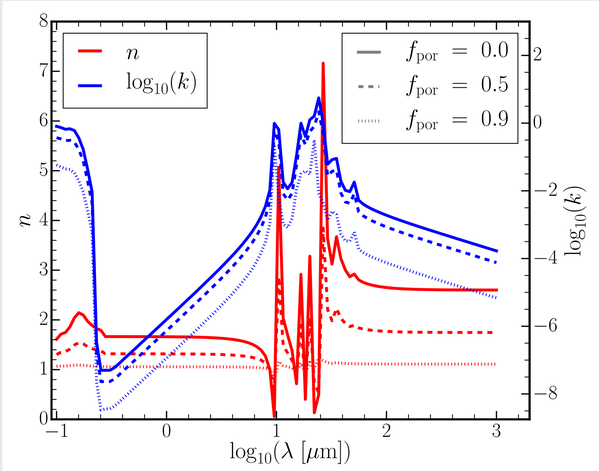

Figure 1: Effects of micro-porosity on real n (red lines, left axis) and imaginary k (blue lines, right axis) refractive indices for a homogeneous Mg_2SiO_4 cloud particle.

We represent non-spherical particle shapes using a distribution of hollow spheres (DHS) [8, 9]. Hollow spheres are composed of a spherical vacuum core and material mantle shell (with radii $a_{\rm core}$ and $a_{\rm mant}$), defined by the parameter $f_{\rm hol}$:

$$f_{\rm hol} = \frac{a_{\rm core}^3}{a_{\rm mant}^3},$$

Non-spherical particle shapes are represented by averaging over a distribution of hollow spheres up to some maximum value, we find $f_{\rm hol}^{\rm max} = 0.85$ to be sufficient [3].

Collisions and Fragmentation of Cloud Particles

We apply a double Dirac delta population distribution with an aggregate population a_1, and a coagulation monomer population a_0 which is set to the average particle size. The aggregate population adjusts to represent the collisional outcomes, based on [10] using the relative timescales of coagulation $\tau_{\rm coag}$, condensation growth $\tau_{\rm grow}$, and settling $\tau_{\rm sett}$. The aggregate size is set by:

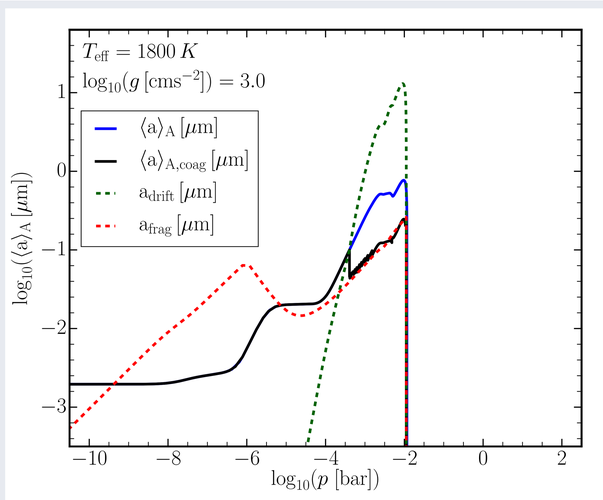

Figure 2: Outcome of double Dirac delta population collision model for 'Typical Warm Gas Giant' ($T_{\rm eff} = 1800\,{\rm K}$, $\log(g\,[{\rm cms^{-2}}]) = 3.0$). Dashed lines show limits to particle growth due to 'rain-out' and fragmentation.

If $a_0 < a_{\rm lim}$:

$$a_1 = \min\left(a_{\rm lim},\ a_0 \exp\left(-\frac{\tau_{\rm sett}}{\tau_{\rm coag}}\right)\right)$$

Or if $a_0 > a_{\rm lim}$:

$$a_1 = \max\left(a_{\rm lim},\ a_0 \exp\left(\frac{\tau_{\rm grow}}{\tau_{\rm coag}}\right)\right)$$

We assume collision velocities generated by turbulence and different settling rates of cloud particles. Limits to aggregate size growth $a_{\rm lim}$ due to 'rain-out' $a_{\rm sett}$ and fragmentation $a_{\rm frag}$. We see that for the 'Typical Warm Gas Giant' that collisions become important at the lower edge of the cloud deck, and that collisions in general fragment cloud particles, leading to a reduction in average cloud particle size.

References

[1] Blecic, J., Harrington, J., Madhusudhan, N., et al. 2014, ApJ, 781, 116
[2] Eylen, V. V., Kjeldsen, H., Christensen-Dalsgaard, J., & Aerts, C. 2012, Astronomische Nachrichten, 333, 1088
[3] Samra, D., Helling, C., & Min, M. 2020, arXiv e-prints, arXiv:2004.13502
[4] Helling, C., Iro, N., Corrales, L., et al. 2019, A&A, 631, A79
[5] Helling, C., Kawashima, Y., Graham, V., et al. 2020, arXiv e-prints, arXiv:2005.14595
[6] Bohren, C. F. & Huffman, D. R. 1983, Absorption and scattering of light by small particles
[7] Bruggeman, D. A. G. 1935, Annalen der Physik, 416, 636
[8] Min, M., Hovenier, J. W., & de Koter, A. 2005, A&A, 432, 909
[9] Min, M., Ormel, C. W., Chubb, K., Helling, C., & Kawashima, Y. 2020, arXiv e-prints, arXiv:2006.12821
[10] Birnstiel, T., Klahr, H., & Ercolano, B. 2012, A&A, 539, A148
[11] Fortney, J. J. 2005, MNRAS, 364, 649

Micro-porosity for a 'Typical Warm Gas Giant'

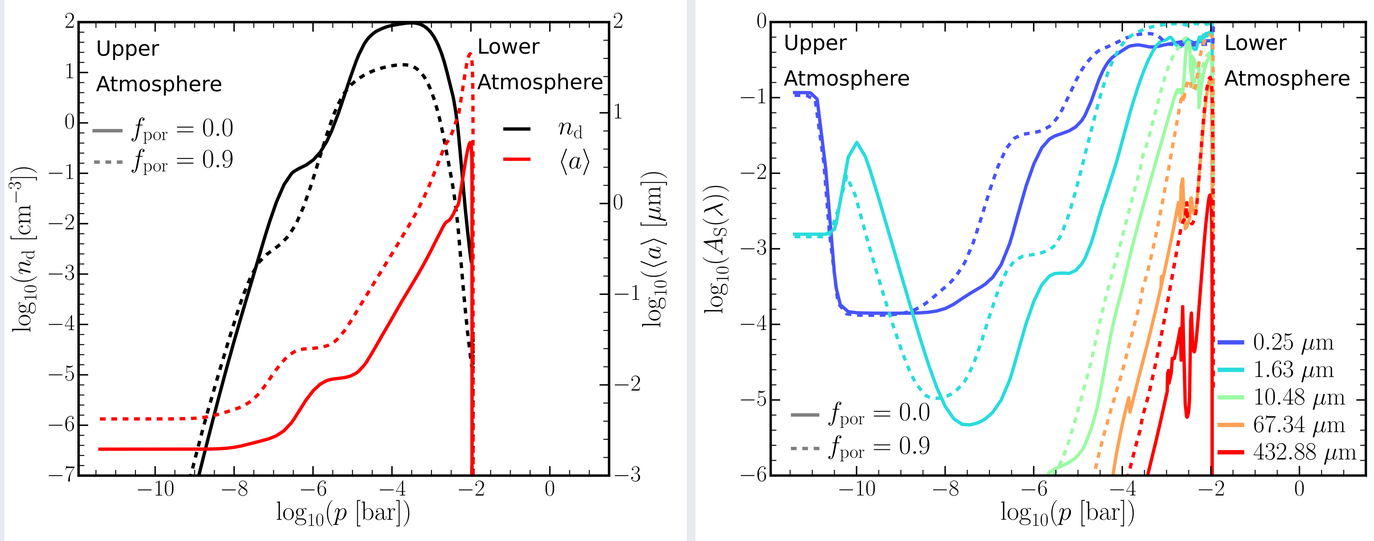

Figure 3: Compact and micro-porous cloud particle properties ($f_{\rm por} = 0.0$ and 0.9 respectively). For a 1D 'typical warm gas giant' DRIFT-PHOENIX atmospheric profile ($T_{\rm eff} = 1800\,{\rm K}$, $\log(g\,[{\rm cms^{-2}}]) = 3.0$). **Left:** Cloud particle number density $n_{\rm d}$ (black lines, left axis) and average size $\langle a \rangle$ (red lines, right axis). **Right:** Single scattering albedo $A_{\rm S}(\lambda) = Q_{\rm sca}(\lambda)/Q_{\rm ext}(\lambda)$ (see figure for wavelengths).

Micro-porosity increases cloud particle surface area. This enables efficient bulk growth and thus reduces peak nucleation rates, leading to larger but less numerous cloud particles. Single scattering albedo is enhanced due to larger cloud particle sizes and changes to material composition. These effects are robust across a range of effective temperatures and surface gravities [3].

Hollow Spheres on HAT-P-7b and WASP-43b

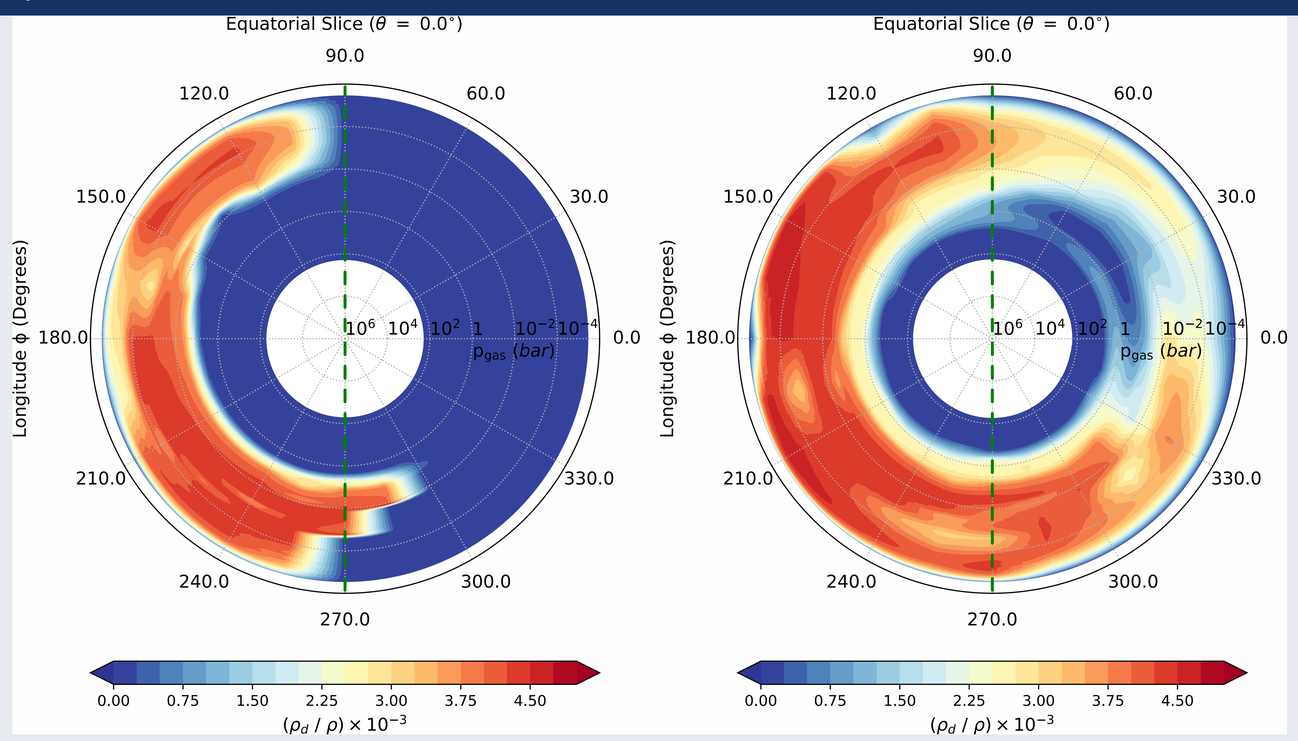

Figure 4: Ratio of cloud particle mass to gas mass $\rho_{\rm d}/\rho$. for slices through the equator ($\theta = 0.0°$) of HAT-P-7b (**left**) and WASP-43b (**right**). $\phi = 0.0°$ is the sub-stellar point. The terminator is indicated by green dotted lines.

Cloud formation traces cooler temperatures. HAT-P-7b hotter on dayside due to irradiaton, so clouds only on the nightside. Clouds more efficient on nightside but also found globally for WASP-43b. Cloud formation is also asymmetric at the terminators for both, as a result of heat re-distribution from the dayside to the nightside.

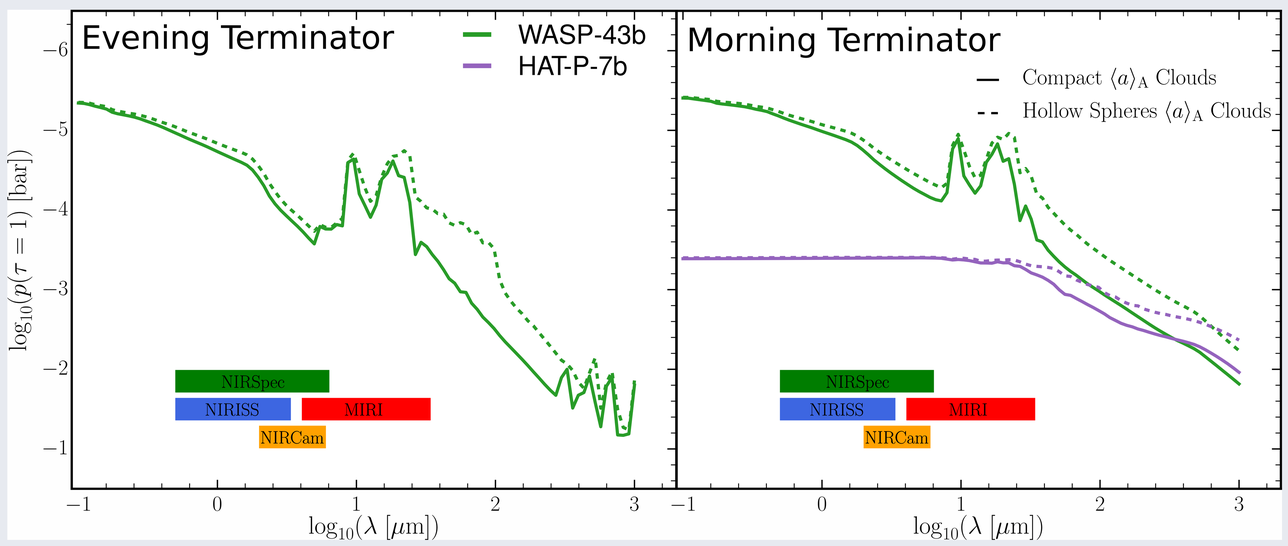

Figure 5: Pressure where the slant integrated optical depth reaches unity for the evening and morning terminators of HAT-P-7b (purple) and WASP-43b (green) at the equator ($\theta = 0.0°$). For both spherical cloud particles (solid) and irregular particle shapes by a DHS (dashed).

Optical depths integrated in a slant geometry [11] for the terminators of WASP-43b display an asymmetry in cloud formation. HAT-P-7b evening terminator does not appear as there are no clouds. Silicate spectral features observable in the MIRI and NIRSPEC wavelength ranges and are affected by irregular cloud particles.

Conclusions

- 'Mineral Snowflakes' affect material and optical properties for porosities of $f_{\rm por} = 0.9$.
- For the 'Typical Warm Gas Giant' cloud particle collisions due to turbulence produce fragmentation, reducing average particle size
- Clouds inhomogeneous around gas-giant and ultra-hot exoplanets due to temperature structure, causing an asymmetry in optical depth of clouds at the terminators.
- A distribution of hollow spheres well represents non-spherical cloud particles, likely observable by JWST MIRI in transmission spectra.